

A comprehensive classification of galaxies in the Sloan Digital Sky Survey: how to tell true from fake AGN?

R. Cid Fernandes,^{1*} G. Stasińska,² A. Mateus¹ and N. Vale Asari¹

¹*Departamento de Física - CFM - Universidade Federal de Santa Catarina, PO Box 476, 88040-900, Florianópolis, SC, Brazil*

²*LUTH, Observatoire de Paris, CNRS, Université Paris Diderot, 5 Place Jules Janssen, 92190 Meudon, France*

Accepted 2010 December 20. Received 2010 December 15; in original form 2010 August 11

ABSTRACT

We use the $W_{H\alpha}$ versus $[\text{N II}]/H\alpha$ (WHAN) diagram introduced by us in previous work to provide a comprehensive emission-line classification of Sloan Digital Sky Survey galaxies. This classification is able to cope with the large population of weak line galaxies that do not appear in traditional diagrams due to a lack of some of the diagnostic lines. A further advantage of the WHAN diagram is to allow the differentiation between two very distinct classes that overlap in the low-ionization nuclear emission-line region (LINER) region of traditional diagnostic diagrams. These are galaxies hosting a weakly active galactic nucleus (wAGN) and ‘retired galaxies’ (RGs), i.e. galaxies that have stopped forming stars and are ionized by their hot low-mass evolved stars.

A useful criterion to distinguish true from fake AGN (i.e. the RGs) is the value of ξ , which measures the ratio of the extinction-corrected $H\alpha$ luminosity with respect to the $H\alpha$ luminosity expected from photoionization by stellar populations older than 10^8 yr. We find that ξ follows a markedly bimodal distribution, with a $\xi \gg 1$ population composed by systems undergoing star formation and/or nuclear activity, and a peak at $\xi \sim 1$ corresponding to the prediction of the RG model. We base our classification scheme not on ξ but on a more readily available and model-independent quantity which provides an excellent observational proxy for ξ : the equivalent width of $H\alpha$. Based on the bimodal distribution of $W_{H\alpha}$, we set the practical division between wAGN and RGs at $W_{H\alpha} = 3 \text{ \AA}$.

Five classes of galaxies are identified within the WHAN diagram:

- (i) pure star-forming galaxies: $\log[\text{N II}]/H\alpha < -0.4$ and $W_{H\alpha} > 3 \text{ \AA}$;
- (ii) strong AGN (i.e. Seyferts): $\log[\text{N II}]/H\alpha > -0.4$ and $W_{H\alpha} > 6 \text{ \AA}$;
- (iii) weak AGN: $\log[\text{N II}]/H\alpha > -0.4$ and $W_{H\alpha}$ between 3 and 6 \AA ;
- (iv) RGs (i.e. fake AGN): $W_{H\alpha} < 3 \text{ \AA}$;
- (v) passive galaxies (actually, lineless galaxies): $W_{H\alpha}$ and $W_{[\text{N II}]}$ $< 0.5 \text{ \AA}$.

A comparative analysis of star formation histories and of other physical and observational properties in these different classes of galaxies corroborates our proposed differentiation between RGs and wAGN in the LINER-like family. This analysis also shows similarities between strong and weak AGN on the one hand, and retired and passive galaxies on the other.

Key words: galaxies: active – galaxies: evolution – galaxies: statistics – galaxies: stellar content.

1 INTRODUCTION

The goal of a classification scheme is to rationally organize a large collection of objects (animals, plants, books, galaxies) into a fixed number of smaller classes without leaving any object aside, in or-

der to help dealing with this large collection. There are obviously many ways to classify objects, depending on what properties one is mostly interested in. For galaxies, one could, for example, be mainly interested in the morphology (Hubble 1936), colours (de Vaucouleurs 1960), spectral features (Morgan & Mayall 1957) etc. It is not only the considered object properties that change from one classification system to another, but also the philosophies underlying the classification process (hierarchical or non-hierarchical,

*E-mail: cid@astro.ufsc.br

supervised or not supervised, ...) all of which have their advantages and drawbacks. Ideally, a classification scheme should be objective and allow easy incorporation of new objects into pre-defined categories. The last criterion, for instance, is not fulfilled by the classifications using principal component analysis (Sodré & Cuevas 1994; Connolly et al. 1995). Most importantly, the classification scheme must be useful, Hubble’s famous tuning fork being a classical example. Another one is the emission-line classification scheme pioneered by Baldwin, Phillips & Terlevich (1981) (see also Pastoriza 1968), which has been widely used over the last three decades.

The advent of large surveys of galaxies providing extensive collections of homogeneous data sets not easily tractable with conventional methods fostered new classification schemes based on automatic procedures such as neural networks (Folkes, Lahav & Maddox 1996), k-means cluster analysis of entire galaxy spectra (Sánchez Almeida et al. 2010) or on human-eye analysis of galaxy morphology by hundreds of thousands of volunteers, as in the beautiful Galaxy Zoo project (Lintott et al. 2010).

Emission-line classifications of galaxies are among the easiest to carry out (once the emission-line intensities are measured) and allow one to deal with such issues as star formation, chemical composition or nuclear activity. They have, for example, helped to gain insight into the nature of warm infrared galaxies (de Grijs et al. 1992), of luminous infrared galaxies (Smith, Lonsdale & Lonsdale 1998), of galaxies in compact groups (Coziol et al. 1998) or into the connection between active galactic nuclei (AGN) and their host galaxies (Kauffmann et al. 2003). The most famous emission-line diagnostic diagram is that based on the $[\text{O III}] \lambda 5007/\text{H}\beta$ versus $[\text{N II}] \lambda 6584/\text{H}\alpha$ line ratios¹ [dubbed the BPT diagram after Baldwin et al. 1981]. This diagram was built to pin down the main source of ionization in the spectra of extragalactic objects, and became one of the major tools for the classification and analysis of emission-line galaxies (ELGs) in the Sloan Digital Sky Survey (SDSS; York et al. 2000).

As emphasized by Cid Fernandes et al. (2010, hereafter CF10), the BPT diagram leaves unclassified a large proportion of ELGs in the SDSS due to quality requirements on four emission lines. The Kewley et al. (2006) classification is even more demanding, as it requires the intensities of as many as seven lines. To remedy this situation, CF10 have proposed a much more economic diagram that allows one to attain the same objectives using only two lines, $\text{H}\alpha$ and $[\text{N II}]$, which are generally the most prominent in the spectra of galaxies. This is a diagram plotting the $\text{H}\alpha$ equivalent width versus $[\text{N II}]/\text{H}\alpha$, which was dubbed the EWH α n2 diagram in that paper and which we will from now on refer to as the WHAN diagram, for simplicity.² The borderlines between different classes of galaxies in the WHAN diagram were defined by optimal transpositions of the Kauffmann et al. (2003), Stasińska et al. (2006, hereafter S06) and Kewley et al. (2006) borderlines on to the $W_{\text{H}\alpha}$ versus $[\text{N II}]/\text{H}\alpha$ plane.

The categories of ELGs considered by Kauffmann et al. (2003) and Kewley et al. (2006) comprised star-forming galaxies (SF),

Seyferts and LINERs.³ This latter category is supposed to comprise objects hosting low-level nuclear activity. However, as demonstrated by Stasińska et al. (2008, hereafter S08), the LINER region in the BPT diagram also contains galaxies that have stopped forming stars and are actually ionized by the hot low-mass evolved stars (HOLMES) contained in them. This idea is not new. It was already put forward to explain the emission-line spectrum of elliptical galaxies (Binette et al. 1994; Macchetto et al. 1996) and even earlier in different contexts (Hills 1972; Terzian 1974; Lyon 1975; Sokolowski & Bland-Hawthorn 1991). This idea is recently gaining support (Kaviraj 2010; Masters et al. 2010; Schawinski et al. 2010), especially with the detailed study of nearby galaxies (Annibali et al. 2010; Eracleous, Hwang & Flohic 2010; Sarzi et al. 2010). As shown by CF10, when taking into account the ‘forgotten population’ of weak line galaxies, the proportion of such ‘retired galaxies’ (RGs) increases dramatically. It is therefore essential to find ways to distinguish these RGs from truly ‘active’ galaxies, i.e. galaxies which contain a (weak) AGN. This is one of the goals of the present paper.

Our second goal is to link the universe of ELGs with the universe of galaxies without emission lines (often dubbed ‘passive galaxies’, PG). We will see that RGs and PGs are in fact very similar objects.

With our WHAN diagram, we will thus be able to provide a comprehensive classification of all SDSS galaxies, including PGs.

The paper is structured as follows. Section 2 presents the samples of galaxies used to work out our classification and our STARLIGHT data base from which the properties of galaxies that we use are extracted. Section 3 lists the initial definition of galaxy classes: SF, Seyferts, LINERs and PGs. Section 4, the core of this paper, sorts out RGs from AGN among LINER-like galaxies and proposes a practical criterion to identify them. Section 5 describes our comprehensive classification of galaxies based on the WHAN diagram and leading to five classes: SF, strong AGN (sAGN), weak AGN (wAGN), RG and PG. Section 6 examines the star formation histories (SFHs) of galaxies within our new classification scheme, placing RGs in the context of the galaxy population in general. Section 7 discusses the distributions of a series of physical and observed properties in the different galaxy classes, to test the pertinence of our new classification. Finally, Section 8 summarizes our main results.

2 SAMPLES AND DATA PRODUCTS

We draw from the nearly 700 thousand galaxies from the main galaxy sample (Strauss et al. 2002) in the seventh data release of the SDSS (Abazajian et al. 2009). Besides the SDSS data, we make use of a suite of STARLIGHT-derived products available at www.starlight.ufsc.br, like stellar masses, stellar extinctions and the full SFHs (Cid Fernandes et al. 2005). Emission-line properties are measured after subtraction of the underlying stellar component determined with the STARLIGHT fit, as described in Mateus et al. (2006).

Two samples are used throughout this work. The ‘full sample’ (hereafter ‘sample F’) is selected by requiring (i) a signal-to-noise ratio $(S/N) \geq 10$ in the continuum around 4750 Å, (ii) no faulty pixels within ± 15 Å of $\text{H}\alpha$ and $[\text{N II}]$, (iii) $z < 0.17$ to eliminate the few objects at higher redshift which survive the previous criterion

¹ In the remaining of this paper, $[\text{O III}] \lambda 5007$ and $[\text{N II}] \lambda 6584$ will be denoted $[\text{O III}]$ and $[\text{N II}]$, respectively.

² Our WHAN diagram is, in a way, very similar to the $W_{[\text{N II}]}$ versus $[\text{N II}]/\text{H}\alpha$ diagram of Coziol et al. (1998). However, the WHAN diagram is easier to interpret, since it concerns two physically independent quantities, $W_{\text{H}\alpha}$ measuring the amount of ionizing photons absorbed by the gas relative to the stellar mass, while $[\text{N II}]/\text{H}\alpha$ is a function of the nitrogen abundance, of the ionization state and temperature of the gas.

³ In those papers, LINERs should have rather been called ‘galaxies with LINER-like spectra’, given that LINER is the abbreviation of ‘low ionization nuclear emission regions’ (as originally introduced by Heckman 1980), and the SDSS spectra cover much more than the nuclear regions of galaxies.

and (iv) $z > 0.04$ to minimize apertures effects. In total, sample F contains 379 330 galaxies.

Sample V is built from a volume-limited sample satisfying $0.04 < z < 0.095$ and absolute r -band magnitude $M_r < -20.43$, to which we further apply criteria (i) and (ii) above. These latter cuts imply only a 6 per cent reduction, with little loss of completeness at the faint end, so this sample is effectively limited in volume. Sample V comprises 152 749 objects. By choosing $z < 0.095$ we eliminate cases where $H\alpha$ and $[N II]$ fall in a region of strong sky lines, so that criterion (ii) is fulfilled.

These samples fulfil the basic requirements for this work. Condition (i) ensures meaningful spectral fits, necessary for stellar population analysis and the production of templates to aid emission-line measurements, while (ii) ensures that the detection of $H\alpha$ and $[N II]$ (the most important lines in this study) is not hampered by artefacts like bad pixels or sky residuals. At the same time, neither of these samples is biased for or against the presence of emission lines, which allows us to treat systems with strong, weak or no emission lines on an equal footing.

Sample F has the advantage of being more numerous and of extending to lower luminosities, while sample V is more adequate for demographic studies and unbiased comparisons among subsamples. The novelties in this work, namely the criterion to separate true from fake AGN and the resulting revision of conventional spectral taxonomy, are mainly related to the most luminous galaxies, so that, in practise, we could use either sample V or F. In what follows, unless stated otherwise, we use sample V.

3 PRELIMINARY GALAXY CLASSES

We subdivide galaxies into different classes according to their emission-line properties. The first division is among galaxies with and ‘without’ emission lines, denoted ELGs and PGs, respectively.

3.1 Passive galaxies

PGs are defined as those with very weak or undetected emission lines. Galaxies are deemed passive if the equivalent widths (W_λ) of both $H\alpha$ and $[N II]$ fall below 0.5 \AA , a criterion which applies to 19 (20) per cent of sample V (F). Since these are the two strongest optical lines, this criterion automatically implies that other lines will be even weaker in general (e.g. Brinchmann et al. 2004, CF10).

In the literature one often finds PGs and ELGs defined in terms of limits on the S/N_λ of emission lines (e.g. Miller et al. 2003; Brinchmann et al. 2004; Mateus et al. 2006). We consider a W_λ -based criterion more appropriate, as it is based on a more direct measurement of the line strength and less explicitly dependent on the quality of the data. In addition W_λ s have an astrophysical meaning. We emphasize that the adopted limiting value of 0.5 \AA is not really meaningful. As will be seen later, none of the discussion presented in this paper would have changed if had we adopted a slightly different limit. We also note in passing that the denomination ‘passive’ for ‘lineless’ systems is adopted just for compatibility with current nomenclature, with no evolutionary connotation as the word would suggest.

3.2 Emission-line galaxies: SF, Seyferts and LINERs

ELGs are defined as everything else, i.e. any source where either $W_{H\alpha}$ or $W_{[N II]}$ is $\geq 0.5 \text{ \AA}$. Notice that this stretches the definition of an ELG to its limit, since, in extreme cases, only one of $H\alpha$ or $[N II]$

is detected! Sample V (F) has 124 410 (303 194) ELGs, 94 (92) per cent of which have both lines stronger than 0.5 \AA .

ELGs are normally subdivided into SF and AGN-like classes on the basis of diagnostic diagrams involving at least four lines, like the BPT diagram ($[O III]/H\beta$ versus $[N II]/H\alpha$). As shown in CF10, the weakness of either or both of $H\beta$ and $[O III]$ implies that such traditional classification schemes leave large numbers of ELGs unclassified. This problem is particularly severe in the right wing of the BPT diagram, where AGN-like systems reside, but well over half of the galaxies have unusable $H\beta$ and/or $[O III]$ fluxes. In that same paper we introduced alternative diagnostic diagrams able to cope with galaxies with weak or undetected $H\beta$ and/or $[O III]$, the most economic of which is $W_{H\alpha}$ versus $[N II]/H\alpha$ (WHAN diagram). We base all our classifications on this diagram, which, unlike any other, allows us to classify all galaxies.

The WHAN diagram is shown in Fig. 1. The vertical line at $\log[N II]/H\alpha = -0.40$ corresponds to the optimal transposition of the S06 BPT-based SF/AGN division, designed to differentiate sources where star formation provides all ionizing photons from those where a harder ionizing spectrum is required. Similarly, the division at $W_{H\alpha} = 6 \text{ \AA}$ represents an optimal transposition of the Kewley et al. (2006) division between Seyferts and LINERs on the basis of seven emission lines. Unlike Kewley et al. (2006) and other studies (e.g. Kauffmann et al. 2003; Mateus et al. 2006), we do not define a ‘SF+AGN composite’ category, and so our Seyfert/LINER borderline goes all the way to the SF/AGN frontier. (The reader is referred to CF10 for a discussion of the pros and cons of this diagram, as well as for a discussion of why we prefer not to define a composite category.) Sample V splits into percentage fractions of 23, 21 and 37 SF, Seyferts and LINERs, respectively.

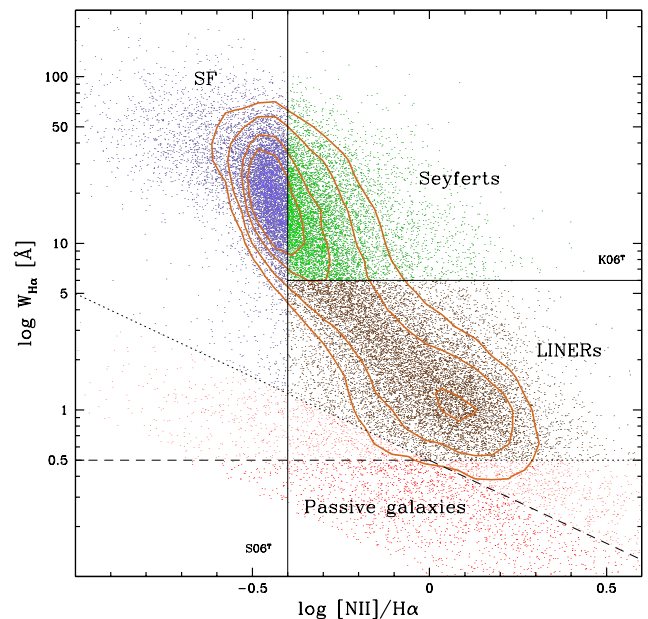


Figure 1. The WHAN diagram, used to establish emission-line classes. The line labelled S06^T represents the optimal transposition of the S06 SF/AGN spectral classification scheme, while the line at $W_{H\alpha} = 6 \text{ \AA}$ represents the transposed version of the Kewley et al. (2006) Seyfert/LINER class division. Dotted lines mark $W_{H\alpha} = 0.5$ and $W_{[N II]} = 0.5 \text{ \AA}$ limits, below which line measurements are uncertain. Passive galaxies ($W_{H\alpha}$ and $W_{[N II]} < 0.5 \text{ \AA}$; red dots) lie below the dashed line. Dots correspond to sample V and contours to sample F. Contours are drawn at number densities: 0.1, 0.2, 0.4 and 0.6 of the peak value. As in other figures in this paper, only one-tenth of the objects is plotted to avoid overcrowding.

PGs account for the remaining 19 per cent. The corresponding fractions for sample F are very similar: 25, 19, 36 and 20 per cent.

The dotted lines in Fig. 1 correspond to $\min(W_{\text{H}\alpha}, W_{[\text{N II}]}) = 0.5 \text{ \AA}$. Points below these lines (painted in orange or red) are thus very uncertain,⁴ but are nevertheless plotted to remind the reader of the existence of such objects. There is indeed some advantage in including lineless galaxies in an emission-line classification scheme since the absence of emission lines is also an information! The region below the dotted lines includes both ELGs with only one line $\geq 0.5 \text{ \AA}$, as well as PGs (below the dashed lines, in red) for which we have H α and [N II] fluxes in our data base.

4 IDENTIFYING RETIRED GALAXIES

Ideally, splitting ELGs into SF and AGN would separate systems whose emission lines are powered exclusively by young stars from those where accretion on to a central supermassive black hole dominates (or at least contributes to) the ionizing radiation field. However, as reviewed in the introduction, this binary scheme does not account for a third phenomenon: photoionization by HOLMES. These RGs are numerous in large-scale surveys (S08), where they occupy LINER-like locations in the commonly used diagnostic diagrams, and are thus erroneously associated to non-stellar activity.

This section investigates ways of identifying RGs. We start with a theoretically motivated definition, but end up with a very simple empirical criterion to diagnose RGs among ELGs.

4.1 Ionizing photons budget: the ξ ratio

By definition, RGs are systems whose old stellar populations suffice to explain the observed emission line properties. Since we already know that nebulae photoionized by HOLMES cover most regions in intensity ratios diagrams (S08), we shall adopt an operationally simple energy-budget criterion and define RGs as galaxies whose old stellar populations are capable of accounting for all of the observed H α emission.

Let $L_{\text{H}\alpha}^{\text{int}}$ be the intrinsic (extinction corrected) H α luminosity of a galaxy, and $L_{\text{H}\alpha}^{\text{exp}}(t > 10^8 \text{ yr})$ denote the luminosity expected from photoionization by populations older than 10^8 yr . The ratio

$$\xi = \frac{L_{\text{H}\alpha}^{\text{int}}}{L_{\text{H}\alpha}^{\text{exp}}(t > 10^8 \text{ yr})} \quad (1)$$

should thus be able to tell if a galaxy is retired ($\xi \leq 1$) or whether some extra source of ionizing photons is present. Given the orders of magnitude difference between the ionizing photon rates of young and old populations, even tiny amounts of ongoing star formation suffice to swamp the ionizing field produced by HOLMES, leading to $\xi \gg 1$ and to a SF-like emission-line pattern due to the softer ionizing spectrum. Similarly, ξ will also grow above 1 in the presence of an AGN. In fact, as long as a galaxy has enough gas to absorb all $h\nu > 13.6 \text{ eV}$ photons produced within it, ξ should never drop below 1.

This way of identifying RGs was previously employed by S08. In what follows we open up the details and discuss the caveats related to the estimation of ξ .

⁴ Our line fitting code, described in Mateus et al. (2006), only accepts fits with $W_\lambda \geq 0.1 \text{ \AA}$, which produces the empty triangle in the bottom left part of the plot.

4.2 Computation of the expected H α luminosity

Neglecting escape and extinction of Lyman continuum radiation, the denominator in equation (1) becomes

$$L_{\text{H}\alpha}^{\text{exp}}(t > 10^8 \text{ yr}) = \frac{h\nu_{\text{H}\alpha}}{f_{\text{H}\alpha}} Q_{\text{H}}^{\text{exp}}(t > 10^8 \text{ yr}), \quad (2)$$

where $f_{\text{H}\alpha} = 2.206$ for case B hydrogen recombination, and $Q_{\text{H}}^{\text{exp}}$ is the expected ionizing photon rate. The STARLIGHT spectral decomposition in terms of a base of simple stellar populations (SSPs) allows us to estimate $Q_{\text{H}}^{\text{exp}}$ for each of our galaxies. The code returns the mass associated to each of N_\star SSPs of different ages (t) and metallicities (Z), so that the expected flux of ionizing photons from the populations of interest here is simply

$$Q_{\text{H}}^{\text{exp}}(t > 10^8 \text{ yr}) = M_\star \sum_{j: t_j > 10^8 \text{ yr}} \mu_j q_{\text{H},j}, \quad (3)$$

where M_\star is the total stellar mass formed, μ is the mass-fraction population vector and $q_{\text{H},j} = q_{\text{H}}(t_j, Z_j)$ is the number of H ionizing photons emitted per unit time and initial mass for the j th SSP. Since the expected H α luminosity is to be compared to the one observed within the 3-arcsec aperture of the SDSS spectroscopic fibre, the stellar mass in this equation corresponds to that inside the fibre (i.e. we do not extrapolate to account for the whole galaxy). In fact, all our analysis up to Section 6 uses within-the-fibre data only.

The STARLIGHT fits used in this work employ the same base of SSPs from Bruzual & Charlot (2003, hereafter BC03) described by Mateus et al. (2006). Naturally, the spectral fits are carried out in the optical range, but the BC03 models also provide predictions for the ionizing energies. This is a key element of our analysis, so it is worth to open a parenthesis to examine these predictions more closely.

4.3 SSP models beyond 1 Rydberg

Fig. 2 shows the evolution of SSP properties of interest to this work. Panels on the left (a–d) correspond to BC03 models of six different metallicities used in our analysis. These are discussed first.

Fig. 2(a) shows the evolution of the hardness of the ionizing spectrum, as measured by the ratio of He I to H I ionizing photons. The difference between the soft ionization field produced by OB stars ($t < 10^7 \text{ yr}$) and that produced by HOLMES is clearly visible. Panel (b) shows the specific ionizing photon rate, $q_{\text{H}}(t, Z)$, the most relevant quantity for our analysis. One sees the well-known drop by ~ 5 orders of magnitude in q_{H} from the H II region phase to the time when the HOLMES regime sets in at 10^8 yr and q_{H} approximately stabilizes at a level of the order of $10^{41} \text{ s}^{-1} \text{ M}_\odot^{-1}$. The specific continuum around H α , $c_{\text{H}\alpha}$ (equivalent to the inverse of the mass to light ratio, $\kappa_{\text{H}\alpha}$), however, keeps decreasing with time (panel c) and therefore the predicted $W_{\text{H}\alpha}$ (bottom panel) goes through a minimum at 10^8 yr and grows to $1.5\text{--}2.5 \text{ \AA}$ at $t \gtrsim 10^{10} \text{ yr}$. This is enough to explain a significant proportion of the ELGs in the LINER zone of Fig. 1.

The right-hand column of Fig. 2 shows the predictions obtained for other evolutionary synthesis models at solar metallicity and Chabrier (2003) initial mass function (IMF; the same one used for the BC03 models on the left-hand panels). Red lines show results for a preliminary version of Charlot & Bruzual models. Blue lines are used for Popstar models (Mollá, García-Vargas & Bressan 2009) with the Lejeune, Cuisinier & Buser (1997) library and NLTE

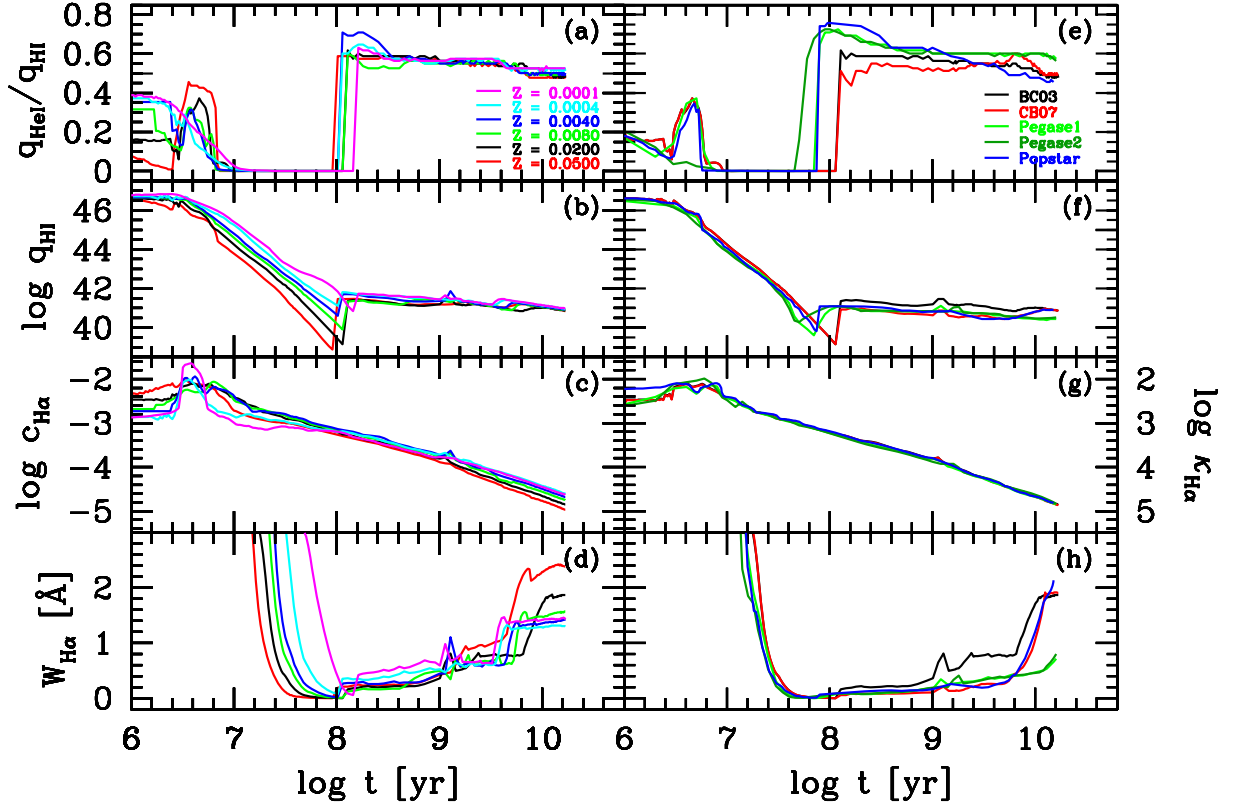


Figure 2. Evolution of the ratio between the He I and H I ionizing photon rates (a), H I ionizing photon rate (b; in units of $s^{-1} M_{\odot}^{-1}$), H α continuum (c; in units of $L_{\odot} \text{ \AA}^{-1} M_{\odot}^{-1}$) and H α equivalent width (d) for simple stellar populations in the BC03 models of metallicities between $Z_{\star} = 0.005$ and $2.5 Z_{\odot}$. Panels on the right are Z_{\odot} models from five different sources (including BC03 for comparison). See text for details. The right axis scale in panels (c) and (g) gives the mass-to-light ratio in the H α continuum: $\kappa_{H\alpha} = c_{H\alpha}^{-1}$ (in units of $M_{\odot} L_{\odot}^{-1} \text{ \AA}$).

models by Rauch (2003) and ‘Padova 1994’ tracks (version updated by Mollá & García-Vargas 2000). Green lines represent Pegase models (Fioc & Rocca-Volmerange 1997) with their 200 \AA –10 μm stellar library (see their section 2.2.1 for more details). Two sets of evolutionary tracks are shown for Pegase: light green is used for Bressan et al. (1993) tracks up to thermally pulsing asymptotic giant branch (TP-AGB), dark green shows the set for Schaller et al. (1992) and Charbonnel et al. (1996) tracks. Both sets use Schoenberner (1983) and Bloeker (1995) for the post-asymptotic giant branch (PAGB). For reference, the BC03 predictions for Z_{\odot} are repeated (black lines).

Despite a general qualitative agreement, there are significant quantitative differences. For ages above 10^8 yr, the hardness ratio varies from 10 to 20 per cent, while q_H differs by up to 1 dex from one model to another. Those differences could be due to differences in stellar tracks, model atmospheres and even interpolation techniques. For $W_{H\alpha}$, the greatest difference is above 10^9 yr for the BC03 models, which are $\sim 0.5 \text{ \AA}$ larger than the others. We have also compared different IMFs (e.g. Salpeter 1955; Kroupa 2001). For a given metallicity in a model, different IMFs result in variations from 0.2 up to 0.5 dex in q_H and $c_{H\alpha}$, which is typically of the same order of variations for different models with the same IMF.

For the sake of internal consistency with our STARLIGHT analysis of SDSS galaxies, in what follows we adopt the predictions from BC03, but this quick compilation illustrates that there are still plenty of uncertainties in model predictions for the Lyman continuum of old stellar populations. Naturally, these uncertainties

propagate to our estimate of ξ . Fortunately, there is an empirical alternative to circumvent the uncertainties related to this choice (Section 4.8).

4.4 Extinction correction

Let us now turn to the numerator of equation (1). The caveat in this case is that a nebular extinction is needed to correct $L_{H\alpha}^{\text{obs}}$ to $L_{H\alpha}^{\text{int}}$, which in turn requires good measurements of both H α and H β . While this is not a problem for ELGs in the SF and Seyfert categories, most of the LINER-like systems do not comply with this requirement because of their feeble H β .

One way to circumvent this difficulty is to estimate H α /H β in terms of something else. To do this, we first select LINERs with reliable H α /H β , and then calibrate the relation between nebular (A_V^{neb}) and stellar (A_V^{\star}) extinctions (as done by Asari et al. 2007 for SF galaxies), such that A_V^{\star} can be used to estimate A_V^{neb} . In practice, we impose $W_{H\alpha}$ and $W_{H\beta} > 0.5 \text{ \AA}$, and H α /H $\beta > 3$ (such that $A_V^{\text{neb}} > 0$),⁵ which leaves us with only ~ 30 per cent of the full list of LINERs. Nebular and stellar extinctions are indeed correlated for this subsample (Spearman rank correlation coefficient $R_s = 0.38$), albeit with substantial scatter. A fit through the median relation yields $A_V^{\text{neb}} = 1.56 A_V^{\star} + 0.53$, with typical residuals of ~ 0.5 mag.

⁵ For the Cardelli, Clayton & Mathis (1989) law used in our analysis, $A_V^{\text{neb}} = 7.215 \log[(H\alpha/H\beta)_{\text{obs}}/(H\alpha/H\beta)_{\text{int}}]$. We adopt an intrinsic Balmer decrement of 3, suitable for LINERs (S08).

Objects used in this calibration have $A_V^{\text{neb}} = 1.0 \pm 0.5$ (median \pm semi-interquartile range), while for LINERs as a whole the above relation leads to $A_V^{\text{neb}} = 0.8 \pm 0.2$. This method most likely overestimates A_V^{neb} , as there is a trend of increasing A_V^{neb} with increasing $W_{\text{H}\alpha}$, and $\text{H}\alpha$ is much weaker in the full sample than in the subset used to calibrate the $A_V^{\text{neb}}(A_V^*)$ relation ($W_{\text{H}\alpha} = 1.5$ versus 3.7 \AA in the median, respectively).

Another alternative is to apply the extinction correction when the data allow ($W_{\text{H}\alpha}$ and $W_{\text{H}\beta} > 0.5 \text{ \AA}$, and $\text{H}\alpha/\text{H}\beta > 3$), and assume $A_V^{\text{neb}} = 0$ otherwise.

These methods lead to estimates of ξ which should bracket the correct solution. Since $A_V^{\text{neb}} = 1$ implies a 0.32 dex increase in $L_{\text{H}\alpha}^{\text{int}}$, for the typical inferred A_V^{neb} values these two methods should differ by ~ 0.2 – 0.3 dex in ξ .

4.5 Results: the bimodal distribution of ξ

The ξ values derived range from ~ 0.1 to 1000. This is illustrated in Fig. 3(a), which shows the distribution of ξ values for all ELGs in sample V. The distribution is strongly bimodal, with a high ξ peak at ~ 30 and a lower one centred close to $\xi = 1$.

The two histograms in Fig. 3(a) differ in the recipe to correct $L_{\text{H}\alpha}^{\text{obs}}$ for extinction when $\text{H}\alpha/\text{H}\beta$ is unreliable. The dotted curve is

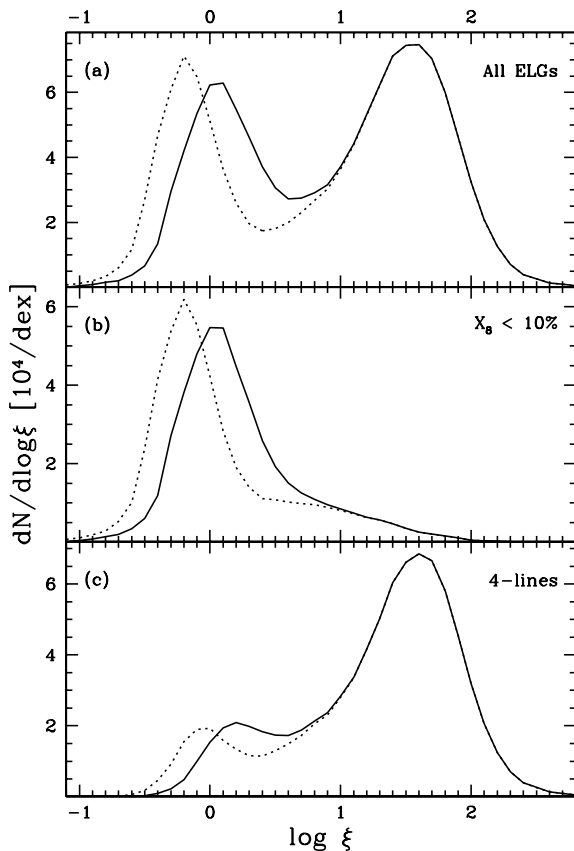


Figure 3. Histograms of the ratio between the intrinsic $\text{H}\alpha$ luminosity $L_{\text{H}\alpha}$ to that predicted to originate from photoionization by HOLMES (equation 1) for ELGs in our volume-limited sample, and for two choices of extinction correction for objects with unreliable $\text{H}\alpha/\text{H}\beta$: estimate A_V^{neb} from A_V^* (solid lines), and no correction (dotted). Panel (a) includes all sources, while in panel (b) we select galaxies whose populations younger than 10^8 yr contribute less than $X_8 = 10$ per cent to the continuum at $\lambda = 4020 \text{ \AA}$. Panel (c) shows the ξ distribution which results from requiring convincing detections of $\text{H}\beta$ and $[\text{O III}]$, as well as $\text{H}\alpha$ and $[\text{N II}]$.

for no correction, whereas the solid one is for the $A_V^{\text{neb}}(A_V^*)$ method discussed above. The curves are identical for $\xi > 10$ because these are Seyfert and SF galaxies, with $\text{H}\alpha$ and $\text{H}\beta$ fluxes good enough to apply the standard correction. In the low ξ peak the two methods differ by just 0.2 dex on the median, as anticipated. Considering the smallness of this difference and that these recipes are likely to bracket the range of possibilities, we henceforth use the average ξ , whose distribution peaks at $\xi \sim 1$.

Overall, the low ξ population is unbelievably close to the exact prediction for RGs: $\xi = 1$! However, are these galaxies really retired in the sense of not having formed stars for a long while? To answer this question, Fig. 3(b) shows the histograms obtained selecting only galaxies whose populations younger than 10^8 yr contributes no more than $X_8 = 10$ per cent of the light at 4020 \AA .⁶ Clearly, the low ξ peak is made up of galaxies which have formed little or no stars in the past 10^8 yr, in full agreement with the RG scenario of S08.

The width of the RG peak in the ξ distribution (as measured from the one-sided dispersion of its lower half, and assuming that the distribution is symmetric) is $\sigma_{\log \xi} \sim 0.24$ dex for the full ELG sample or 0.13 dex eliminating those with $W_{\text{H}\alpha} < 0.5 \text{ \AA}$. From the considerations in the above sections, one would hardly expect ξ to be more precise than a factor of 2, so that this observed dispersion can be accounted for by uncertainties in the data and the analysis.

While theory says that RGs should have $\xi \leq 1$, the observed bimodality in the ξ distribution suggests that $\xi < 2$ or 3 is a more effective way of separating RGs from the rest of the ELG population (Fig. 3a). About one-third of the full ELG sample has $\xi < 2$. The reason why this huge population of RGs has received little attention to date is because standard selection criteria tend to exclude them from emission line studies. Fig. 3(c) illustrates how the distribution of ξ changes by imposing a $W_\lambda > 0.5 \text{ \AA}$ quality control for the four lines in the BPT diagram: $\text{H}\beta$, $[\text{O III}]$, $\text{H}\alpha$ and $[\text{N II}]$. This reduces the ELG sample as a whole by $\sim 1/3$, but the fraction of $\xi < 2$ sources decreases by a factor of 3. The bimodality is still present, but the low ξ peak is heavily suppressed, so that RGs are the main victims of this cut. With the WHAN diagram we are able to rescue RGs and weak line galaxies in general, eliminating this bias and thus drawing a much more complete view of ELGs in the local Universe.

4.6 Results: ξ versus $[\text{N II}]/\text{H}\alpha$

Fig. 4 shows the results of this analysis in a ξ versus $[\text{N II}]/\text{H}\alpha$ diagram, colour coding SF, Seyferts and LINERs according to their location on the WHAN diagram (Fig. 1). The plot shows that SF, Seyferts and LINERs are well separated in terms of ξ and $[\text{N II}]/\text{H}\alpha$, with SF and Seyferts being responsible for the $\xi \gg 1$ peak and LINERs for the $\xi \sim 1$ RG-like population. The plot also illustrates how dangerous it is to define a galaxy as an AGN on the basis of $[\text{N II}]/\text{H}\alpha$ alone. Miller et al. (2003), for instance, define ‘2-lines AGN’ as sources with $\log[\text{N II}]/\text{H}\alpha > -0.2$ (similar to the ‘low S/N AGN’ in Brinchmann et al. 2004), while our analysis suggests that

⁶ To have an idea of what this means, $X_8 < 10$ per cent corresponds to specific star formation rates (SSFRs) $\lesssim 2.5 \times 10^{-12} \text{ yr}^{-1}$, or, equivalently, to less than 0.025 per cent of the stellar mass having formed in the past 10^8 yr. In fact, for light levels as low as $X_8 = 10$ per cent the spectral synthesis analysis is affected both by its own limitations and by side-effects of incompleteness in evolutionary synthesis models, such that the true contribution from young stars cannot be reliably estimated (see Section 6).

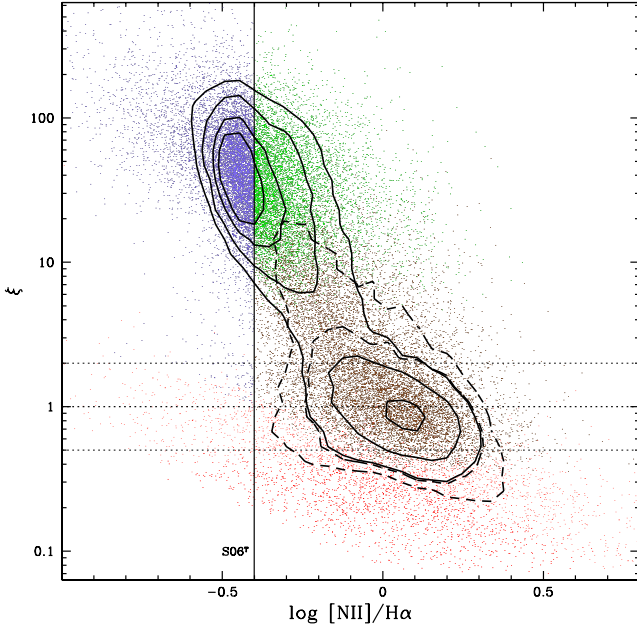


Figure 4. ELGs in the ξ versus $[\text{NII}]/\text{H}\alpha$ diagram, colour coding PGs, LINERS, Seyferts and SF, as in Fig. 1. Also as in Fig. 1, orange points are sources with either or both of $\text{H}\alpha$ and $[\text{NII}]$ weaker than 0.5 \AA . Solid contours are for the full sample V, while the dashed ones are for galaxies with less than $X_8 = 10$ per cent of their flux at $\lambda = 4020 \text{ \AA}$ due to populations younger than 10^8 yr (for clarity, only the two outer contours are plotted in this case). Dotted horizontal lines mark a range of $\times 2$ around the prediction of the RG model ($\xi = 1$).

most of this population does not require an energetically significant non-stellar source of ionizing photons.

The dashed contours in Fig. 4 show the location of ELGs with $X_8 < 10$ per cent. This clarifies that the bulk of the population of large ξ sources among galaxies with a predominantly old stellar population (seen in the middle panel of Fig. 3) is composed of LINERs approaching the Seyferts zone. Further considering that the X_8 cut eliminates sources with significant on-going star formation, this strongly indicates that these sources have a non-stellar source powering most of its line emission (i.e. they are AGN in old hosts).

We note in passing a tiny population of galaxies with small ξ (i.e. consistent with our RG model) but located to the left of the S06 line in Fig. 4. These could correspond low-mass, low-metallicity galaxies in a quiescent phase between bursts of star formation, such as the galaxies discussed by Sánchez Almeida et al. (2008).

4.7 ξ versus $W_{\text{H}\alpha}$

An important aspect of Fig. 4 is its striking similarity to the WHAN diagram of Fig. 1. This happens because ξ and $W_{\text{H}\alpha}$ are very closely related. The equivalent width of $\text{H}\alpha$ is defined as $W_{\text{H}\alpha} = I_{\text{H}\alpha}^{\text{obs}}/C_{\text{H}\alpha}^{\text{obs}}$, where the denominator is the observed continuum luminosity around $\text{H}\alpha$.⁷ Hence, extinction corrections aside, $W_{\text{H}\alpha}$ and ξ (equation 1) have the same numerator.

Because $q_{\text{H}}(t, Z)$ varies little with t or Z after 10^8 yr (Figs 2b and f), and since most of the mass is always in the old populations (over 99 per cent for our samples), $Q_{\text{H}}^{\text{exp}}(t > 10^8 \text{ yr})$ in equa-

tion (3) becomes $\sim M_* q_{\text{H}}^{\text{old}}$, where $q_{\text{H}}^{\text{old}}$, the specific ionizing flux due to HOLMES, is of the order of $10^{41} \text{ s}^{-1} \text{ M}_{\odot}^{-1}$. M_* can be written in terms of the intrinsic continuum at $\text{H}\alpha$ and the galaxy's luminosity weighted mass-to-light ratio: $M_* = C_{\text{H}\alpha}^{\text{int}} \langle \kappa_{\text{H}\alpha} \rangle_L$, where $\kappa_{\text{H}\alpha} = c_{\text{H}\alpha}^{-1}$ was previously discussed in Section 4.3. While $\kappa_{\text{H}\alpha}$ spans nearly three decades for SSPs between 10^6 and 10^{10} yr (Fig. 2c), galaxies are not SSPs, and young (low $\kappa_{\text{H}\alpha}$) populations rarely make a substantial contribution to the $\text{H}\alpha$ continuum, so that the luminosity weighted $\kappa_{\text{H}\alpha}$ values are of the same order for most sources. For the V sample, for instance, $\log \langle \kappa_{\text{H}\alpha} \rangle_L = 4.56 \pm 0.14$ (median \pm semi-interquartile range), while subsamples of SF, Seyferts, LINERs and PGs have 4.35 ± 0.12 , 4.47 ± 0.08 , 4.65 ± 0.08 and 4.70 ± 0.06 , respectively (in units of $\text{M}_{\odot} \text{ L}_{\odot}^{-1} \text{ \AA}$). As a result, $L_{\text{H}\alpha}^{\text{exp}}$ is directly proportional to the $\text{H}\alpha$ continuum, with little scatter due to variations in the SFHs, and thus the denominators of ξ and $W_{\text{H}\alpha}$ essentially measure the same thing.

With these approximations, one finds that

$$\xi = \frac{W_{\text{H}\alpha}}{W_{\text{H}\alpha}^{\text{old}}} 10^{0.4(A_{\text{H}\alpha}^{\text{neb}} - A_{\text{H}\alpha}^{\text{star}})}, \quad (4)$$

where the $A_{\text{H}\alpha}^{\text{neb}} - A_{\text{H}\alpha}^{\text{star}}$ term comes from the fact that ξ accounts for possible differences in the nebular and stellar extinctions, whereas $W_{\text{H}\alpha}$ does not, and

$$W_{\text{H}\alpha}^{\text{old}} \equiv \frac{h\nu_{\text{H}\alpha}}{f_{\text{H}\alpha}} \langle \kappa_{\text{H}\alpha} \rangle_L q_{\text{H}}^{\text{old}} = 0.355 \text{ \AA} \left[\frac{\langle \kappa_{\text{H}\alpha} \rangle_L}{10^4} \right] \left[\frac{q_{\text{H}}^{\text{old}}}{10^{41}} \right] \quad (5)$$

is the expected equivalent width for an old population (for $\langle \kappa_{\text{H}\alpha} \rangle_L$ in units of $\text{M}_{\odot} \text{ L}_{\odot}^{-1} \text{ \AA}$, and $q_{\text{H}}^{\text{old}}$ in $\text{s}^{-1} \text{ M}_{\odot}^{-1}$).

Fig. 5 shows the observed relation between ξ and $W_{\text{H}\alpha}$. The bottom panel (c) shows the dust corrected ξ value. Points in cyan and orange correspond to galaxies where $\text{H}\alpha/\text{H}\beta$ is or is not reliable, respectively. The correlation is very tight, as indicated by the 10 and 90 per cent percentile lines (in dashed). However, the differential extinction correction to ξ creates a hump starting around $W_{\text{H}\alpha} \sim 2 \text{ \AA}$, coinciding with the transition between $\text{H}\alpha/\text{H}\beta$ -based corrections and those based on other methods (see Section 4.4).

Fig. 5(b) shows the same relation assuming that $\text{H}\alpha$ and its continuum are equally affected by dust ($A_{\text{V}}^{\text{neb}} = A_{\text{V}}^{\text{star}}$), so that the last term in equation (4) disappears, and so does the hump in Fig. 5(c). The relation is linear except at high $W_{\text{H}\alpha}$, where it steepens because of the decrease in $\langle \kappa_{\text{H}\alpha} \rangle_L$ in galaxies with lots of star formation. A fit through the median curve in its low $W_{\text{H}\alpha}$ end yields $\log \xi^{\text{obs}} = 1.07 \log W_{\text{H}\alpha} - 0.17$. Forcing a linear fit leads to $W_{\text{H}\alpha}^{\text{old}} = 0.67 \text{ \AA}$. For comparison, this value of $W_{\text{H}\alpha}^{\text{old}}$ is reached for ages of a few Gyr for the BC03 SSPs, or closer to 10 Gyr for other models (bottom panels in Fig. 2).

4.8 Retired galaxies: an empirical diagnostic

This section started with the promise of finding a diagnostic to identify RGs. The ξ ratio was introduced with this purpose, and we have seen that it is indeed capable of capturing in a single number the essence of RGs. However, there are caveats related to this index. First, uncertainties related to the extinction correction affect ξ at a level of $\pm 0.2 \text{ dex}$. Secondly, and far more important, ξ is explicitly dependent on evolutionary synthesis models, whose predictions for the ionizing fluxes from old stellar populations are still plagued by systematic uncertainties (Section 4.3, see also S08). Hence, while it is clear that RGs should populate the bottom of the ξ -scale, theory alone does not allow us to establish a firm upper limit below which a galaxy can confidently be considered as retired. A last caveat is

⁷ $C_{\text{H}\alpha}$ is not to be confused with the continuum luminosity per unit mass, $c_{\text{H}\alpha}$, introduced in Section 4.3. We use capital letters for extensive quantities (like $C_{\text{H}\alpha}$ and Q_{H}), and lowercase for specific ones ($c_{\text{H}\alpha}$ and q_{H}).

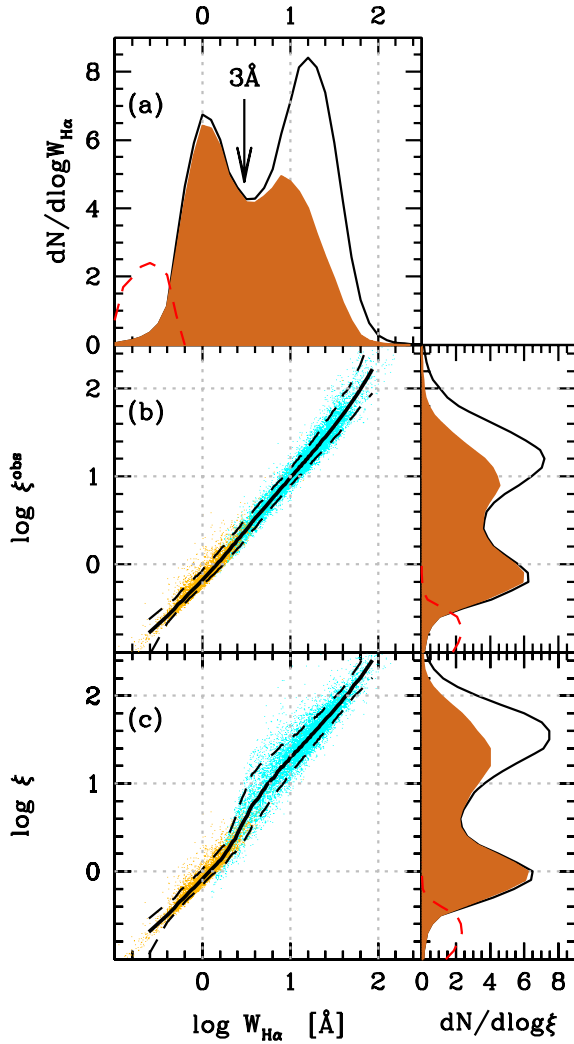


Figure 5. Relation between ξ and $W_{H\alpha}$. The bottom panel (c) shows the average ξ value discussed in Section 4.4, while in the middle panel (b) no extinction correction was applied to $L_{H\alpha}$. Points in cyan (orange) correspond to galaxies where $H\alpha/H\beta$ is (is not) reliable. The black solid line (panels b and c) shows the median relation, while the dashed lines represent the 10 and 90 per cent percentiles. In all projected histograms the black line represents all ELGs, while the filled region represents those with $\log[N II]/H\alpha > -0.4$ (i.e. to the right of the S06^T line in the WHAN diagram), and the dashed red line indicates PGs for which a (necessarily small and uncertain) $H\alpha$ flux is available. The arrow in the $W_{H\alpha}$ distribution marks the proposed limit to separate RGs from other ELGs.

that the evaluation of ξ requires a stellar population analysis, which is not always available or possible.

Fortunately, there is a simple empirical alternative to circumvent these difficulties.

As seen in Fig. 5(a), and in agreement with previous studies (e.g., Bamford et al. 2008), the distribution of $W_{H\alpha}$ is strongly bimodal, with a low peak centred at $W_{H\alpha} = 1 \text{ \AA}$, an upper one at 16 \AA , and an intermediate minimum in the neighbourhood of 3 \AA . This happens both for the sample as a whole and for the subset of AGN-like galaxies, shown by the filled histogram. This bimodality strongly suggests that different mechanisms are at work: photoionization by HOLMES on the low $W_{H\alpha}$ side and by massive stars and/or AGN for large $W_{H\alpha}$. One can therefore use the observed $W_{H\alpha}$ distribution to set an empirical bound for RGs. Of course, the same can be

done for the ξ distribution, but it is clearly advantageous to draw this boundary on the basis of a universally available and model-independent quantity: $W_{H\alpha}$.

We conducted various experiments to define an optimal boundary to separate the two peaks, all giving results between 3 and 4 \AA . We settled for $W_{H\alpha} = 3 \text{ \AA}$. We thus propose to the following practical definition: RGs are ELGs with $W_{H\alpha} < 3 \text{ \AA}$.

For $W_{H\alpha} < 3 \text{ \AA}$, the central black hole may well be active (i.e. accreting), but its ionizing photon output is comparable to or weaker than that produced by HOLMES. For $W_{H\alpha}^{\text{old}}$ values between 1 and 2 \AA , which are compatible with current models (bottom panels in Fig. 2), one finds that at our proposed $W_{H\alpha} = 3 \text{ \AA}$ borderline the AGN contributes between $\sim 1/3$ and $2/3$ of the ionizing power. Naturally, this fraction decreases even more as $W_{H\alpha}$ decreases, to the point that AGN contribution is negligible for the bulk of the low $W_{H\alpha}$ population. It is therefore not correct to use the emission lines of $W_{H\alpha} < 3 \text{ \AA}$ systems to infer AGN properties.

5 A COMPREHENSIVE CLASSIFICATION OF GALAXIES

We are now able to separate fake AGN (= RGs) from true AGN. In the LINER zone of Fig. 1, true AGN are defined by $3 < W_{H\alpha} < 6 \text{ \AA}$. To avoid confusion, we shall call these sources ‘wAGN’. In the interest of a consistent notation, we shall also rename Seyferts as ‘sAGN’. Finally, we remove from the SF category those galaxies consistent with a RG classification, that is to say those having $W_{H\alpha} < 3 \text{ \AA}$.

Our final classification scheme is shown in Fig. 6. Sample V sources split into percentage fractions of 22, 21, 8, 31 and 18 SF, sAGN, wAGN, RG and PG, respectively. RGs therefore exist in large numbers in the SDSS, in agreement with the basic prediction that such systems are bound to exist as a mere consequence of stellar evolution. AGN, on the other hand, are far less common than one would infer associating all LINERs to non-stellar activity.

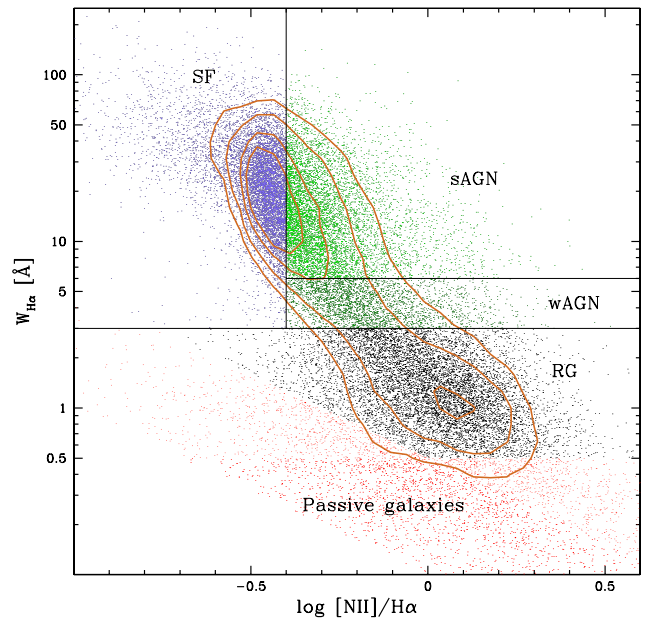


Figure 6. The WHAN diagram with the revised categories: SF, sAGN, wAGN, RGs and PGs. Points with one of $[N II]$ or $H\alpha$ weaker than 0.5 \AA are plotted in orange, except for PGs, which are plotted in red.

This revised classification scheme has three main virtues.

- (i) It identifies the three main ionizing agents in galaxies: young stars, AGN and HOLMES.
- (ii) It is based on the cheapest and therefore most inclusive diagnostic diagram, the only one able to handle the huge population of weak line galaxies (CF10). In fact, it even allows us to visualize a region occupied by PGs, something which is not possible in conventional intensity ratio diagnostic diagrams (of course, galaxies with no emission lines at all do not appear in this diagram).
- (iii) The SF/AGN and wAGN/sAGN frontiers are based on optimal transpositions of widely used demarcation lines defined on the basis of traditional diagnostic diagrams, such that the WHAN diagram preserves traditional classification schemes where they work well, while at the same time fixing their inability to deal with weak line galaxies and to distinguish true from fake AGN.

Before exploring the realm of galaxies under the perspective of this new classification scheme, a few clarifications are in order.

First, notice that our SF/AGN borderline corresponds to the transposition of the S06 BPT-based criterion to isolate systems powered exclusively by young stars from those where a harder ionizing source is required. As such, it would have been better to call it a ‘pure-SF’ demarcation line, instead of a ‘SF/AGN’ divisory line. This is all the more true now that we realize that the AGN-like population of ELGs in the BPT is full of RGs whose black holes are not active enough to affect their emission lines.

Secondly, notice that the $W_{H\alpha} < 3 \text{ \AA}$ criterion slightly modifies our idealized definition of RGs as ‘systems whose old stellar populations suffice to explain the observed emission-line properties’ (Section 4.1) to one where HOLMES make at least a substantial contribution to the ionizing field. Such a fuzzy frontier is unavoidable. Our criterion is designed to avoid RGs being misclassified as AGN. On the other hand, some galaxies hosting an AGN, particularly those containing a weakly active nucleus, may drift to the $W_{H\alpha} < 3 \text{ \AA}$ zone if observed within an aperture larger than the SDSS 3 arcsec spectroscopic fibre.

Numerical experiments show that this is indeed likely to happen. Picking the $H\alpha$ luminosity of a randomly chosen AGN and adding it to the spectrum of a random bona fide RG with $W_{H\alpha}$ within $1 \pm 0.5 \text{ \AA}$, we find that about one-third of the resulting simulated spectra have $W_{H\alpha} < 3 \text{ \AA}$, most of which in the $2\text{--}3 \text{ \AA}$ range. We thus expect that a fraction of the systems here classified as RGs turn out to harbour wAGN when looked up more closely. At first sight, this seems to be a drawback of using $W_{H\alpha}$ for spectral classification, but it is not. After all, if an AGN is present and yet $W_{H\alpha} < 3 \text{ \AA}$, then it is still correct to infer that old stars make a substantial contribution to the observed line emission.

Finally, we note that the division of AGN into strong and weak categories on the basis of $W_{H\alpha}$ is also to some extent aperture dependent, since sAGN may be diluted to wAGN as more stellar continuum is sampled. This, however, is a minor issue, since both classes are clearly AGN-dominated systems, so there is no risk of misidentifying the dominant ionizing agent.

6 THE STAR FORMATION HISTORIES WITHIN OUR CLASSIFICATION SCHEME

A popular approach to digest the flood of information from mega surveys like the SDSS is to compare the properties of galaxies in different classes (SF versus AGN, Seyfert versus LINER, early versus late type, field versus cluster etc.), in search of clues which may help understanding why galaxies are the way they are (see Blanton

& Moustakas 2009 for examples of studies following this general strategy). Taxonomy, of course, plays a central role in such comparative studies. In this section we present yet another comparative study, but this time following the new taxonomical framework proposed in the previous section and summarized in Fig. 6. The main novelty in this scheme is the introduction of the RG category, whose members were previously misclassified as AGN. A major goal of this section is to place RGs in the context of the galaxy population in general, which was never done before. On the one hand, we want to compare RGs with other ELGs, especially wAGN, with which RGs were so far confused. It is also interesting to compare wAGN to sAGN, since this division was merely introduced for the sake of ‘backwards compatibility’ with the historical Seyfert/LINER subdivision of AGNs. On the other hand, it is equally important to compare RGs and PGs. According to the RG concept, galaxies without emission lines should not exist, since HOLMES provide a minimum floor ionizing field capable of powering emission lines. Seen from this perspective, the existence of PGs raises questions like: Are they truly lineless systems or is it just an issue of detectability? Perhaps PGs lack the warm/cold ISM to reprocess ionizing photons?

The STARLIGHT–SDSS data base offers plenty of material for this comparative study. In what follows we use a suite of physical properties as well as the detailed SFHs to address the issues raised above. Only the volume-limited sample is used from here on.

An instructive way to start this comparative study is to investigate how SFHs vary as a function of the SF/sAGN/wAGN/RG/PG spectral types defined in Fig. 6. This is done in Fig. 7 where we chopped the WHAN diagram in 0.2×0.3 dex wide bins in $[\text{N II}]/H\alpha$ and $W_{H\alpha}$. In each box we plot the time-dependent median of the SSFR for galaxies in the box, colour coding the curves according to the Fig. 6 emission-line taxonomy. The SSFR(t) functions were smoothed exactly as in Asari et al. (2007), which should be consulted for details

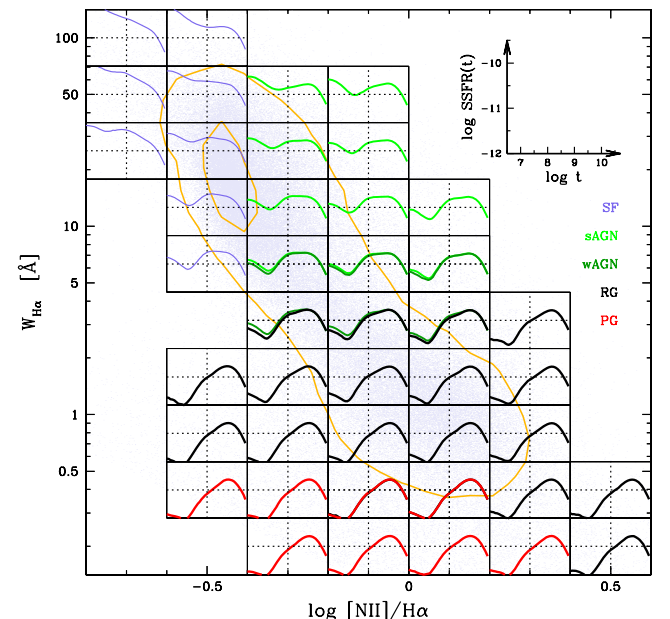


Figure 7. SFHs as a function of spectral class and the location in the WHAN diagram. Each box shows the median SSFR(t) for galaxies of different types, coded by different colours. The scale of these plots is shown in the inset. Curves are only drawn for boxes containing over 200 galaxies. Only galaxies in the volume-limited sample are used in this plot. Contours correspond to 0.1 and 0.6 of the peak density.

on how this and other representations of STARLIGHT-based SFHs are derived.

Because this is our classification diagram, most boxes contain only one curve, with exceptions at locations straddling the nominal frontier between RGs and wAGN (at $W_{\text{H}\alpha} = 3 \text{ \AA}$) and wAGN/sAGN ($W_{\text{H}\alpha} = 6 \text{ \AA}$). Although there are strong systematic changes in SFHs across this plane, in these borderline cases one sees little difference between the SFHs of two adjacent classes.

Several trends are visible in Fig. 7. For instance, focusing on the column centred at $\log[\text{N II}]/\text{H}\alpha = -0.1$, one sees that both PGs and RGs have SFHs concentrated in the largest ages, while, moving upwards the retrieved SFHs reveal increasing levels of recent star formation. Because of the large apertures covered by the SDSS fibres, most of the $\text{H}\alpha$ emission in these AGN probably comes from star formation rather than the AGN (e.g. Kauffmann et al. 2003), so the increase in recent SSFR with $W_{\text{H}\alpha}$ is expected. However, the effect of the AGN is present, as can be inferred by the decreasing levels of recent SSFR towards the right for fixed $W_{\text{H}\alpha}$ (best visible in the rows centred at $W_{\text{H}\alpha} \sim 10 \text{ \AA}$).

Before we proceed, a parenthesis must be opened to clarify the meaning of the small upturn in $\text{SSFR}(t)$ at $t \lesssim 10^7 \text{ yr}$ for RGs and PGs. This feature is almost certainly an artefact of incomplete modelling of the horizontal branch phase (Koleva et al. 2008; Cid Fernandes & González Delgado 2010; Ocvirk 2010). This effect was quantified by Ocvirk (2010), who estimates that these ‘fake young bursts’ account for up to 12 per cent of the recovered optical light fractions in spectral synthesis of genuinely old stellar populations. In units of the SSFR, this corresponds to a few times 10^{-12} yr^{-1} , which is precisely the level at which upturns at small ages are seen in Fig. 7. We further find a clear trend for this artefact to be related to the stellar metallicity, with the low t hump increasing for decreasing Z_* , in agreement with the fact that bluer horizontal branches occur for lower Z_* (Harris 1996; see also Fig. 8 for indirect evidence of this trend). Finally, if the upturn were really due to young stars, $W_{\text{H}\alpha}$ should be much larger than observed. Including these fake young bursts in the predictions for the ionizing flux leads to (in the median)

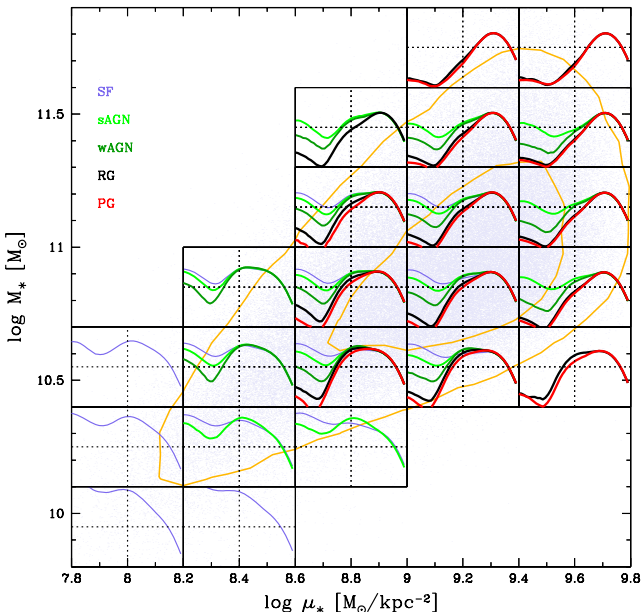


Figure 8. As Fig. 7, but in the plane defined by the mean stellar surface density and stellar mass. μ_* is computed dividing half the stellar mass by the radius which contains half the z -band light.

expected $W_{\text{H}\alpha}$ values over three times as large as observed for RGs. The overprediction for PGs is even worse, with a median expected $W_{\text{H}\alpha}$ of 3.2 \AA , while their definition requires $W_{\text{H}\alpha} < 0.5 \text{ \AA}$.

Credible levels of recent star formation only appear for boxes centred at $W_{\text{H}\alpha} \geq 3 \text{ \AA}$ in Fig. 7, coinciding with the RG/wAGN transition. This suggests that all AGN are associated to at least some level of ongoing star formation. While this is well known and documented for sAGN (the so-called ‘starburst–AGN connection’) the situation is much less clear for wAGN (e.g. González Delgado et al. 2004 and references therein). It is difficult to compare this finding with those in previous studies because of varying definitions of wAGN, but we can confidently say that the signatures of star formation in wAGN identified in this work would be wiped out without removing the RGs from the AGN category.

We now investigate how SFHs vary in terms of properties not explicitly involved in the definition of our spectral classes. Fig. 8 shows SFHs in a stellar mass (M_*) versus mass density (μ_*) diagram. This allows us to compare the SFHs of galaxies which are similar in terms of global properties, but differ in terms of emission-line properties, since this time each box can contain galaxies of different classes. Again, several trends are evident to the eye. One of them is the signature of downsizing, here manifested by the decrease in recent SSFR levels as one moves up the mass scale, seen, for instance, in the curves for SF galaxies in the first two columns of boxes. A similar behaviour is also seen for RGs and PGs,⁸ but shifted in time to $t \sim 10^9 \text{ yr}$.

For this study, the more relevant trend in Fig. 8 is that in every box the lines corresponding to our different classes appear in the same order, with recent star formation decreasing from SF galaxies to sAGN, wAGN, RGs and PGs. These last two, in fact, have median SFHs which are very similar and sometimes indistinguishable. Both types retired from forming stars over 10^8 yr ago. The plot also shows that the recent SSFR of wAGN never reaches levels as low as those of RGs and PGs. Despite their generally low levels of star formation compared to sAGN of same M_* and μ_* , wAGN are not retired, reinforcing the idea that star formation and AGN activity are connected even in the weakest cases, at least in a statistical sense.

Fig. 9 shows another example. The plot shows the observational colour–magnitude diagram, with the familiar red sequence, blue cloud and green valley pattern. This diagram is meant to provide an empirical representation of the age–mass relation. As expected, systems in the blue cloud are more actively forming stars nowadays than in their past average, while red sequence galaxies (with the exception of AGN) tend to be retired. Again, the SF to PG sequence in levels of recent SSFR and the similarity between RGs and PGs seen in Figs 7 and 8 is present in every box.

In summary, the extended emission-line classification scheme proposed here bears an excellent correspondence with the SFHs of galaxies. RGs and PGs have very similar SFHs for similar global properties. wAGN are more similar to sAGN in terms of SFHs than to RGs or PGs. Traditional classification schemes which ignore RGs, would, on the contrary, find wAGN to be more like PGs.

⁸ Recall that the ‘mini bursts’ at $t \lesssim 10^7 \text{ yr}$ are not real, but artefacts of spectral fits with an incomplete base (Ocvirk 2010). The fact that these fake bursts correlate with galaxy mass, as seen in Fig. 8, is likely an indirect consequence of the connection between horizontal branch morphology and Z_* coupled to the M_* – Z_* relation.

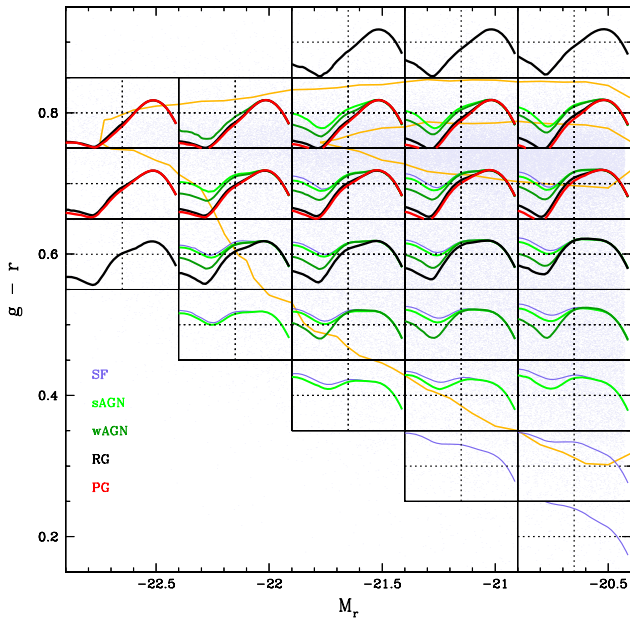


Figure 9. As Fig. 7, but for the observational colour–magnitude diagram.

7 DISTRIBUTIONS OF GLOBAL GALAXY PROPERTIES

Comparing the distributions of global properties of different galaxy classes can provide a further test of the pertinence of our classification scheme. This is done in Fig. 10 that shows normalized histograms of PG, RG, wAGN, sAGN and SF galaxies in terms of a series of properties related to their structure, stellar populations, gas and dust content.

A striking feature of these histograms is that for most properties PG and RG have similar distributions, reinforcing our interpretation that PG and RG are essentially the same thing, or at least that these classes overlap heavily. On the other hand, the distributions for wAGN are more similar to the ones of sAGN, suggesting that these galaxies belong to the same family. This is a salutary a posteriori validation of our splitting of LINERs into two very different classes: RGs and wAGN.

Except for SF galaxies, all other galaxy types have masses within roughly ± 0.5 dex of $10^{11} M_{\odot}$ (Fig. 10a). This is mostly due to the luminosity cut for the V sample, which imposes a mass completeness limit of $\sim 10^{10.8} M_{\odot}$. In the median, $M_{\star}^{\text{sAGN}} < M_{\star}^{\text{wAGN}} \sim M_{\star}^{\text{PG}} < M_{\star}^{\text{RG}}$. In terms of surface densities and velocity dispersions (Figs 10b and c), PGs and RGs are statistically similar, occupying the high end of the distributions. Despite the substantial overlap, it is clear that wAGN and sAGN tend to have smaller σ_{\star} and μ_{\star} than RGs and PGs. The same is true for the escape velocity, computed from $(GM_{\star}/R)^{1/2}$ with R given by the half-light z -band radius (Fig. 10d). PGs and RGs also differ from AGN in terms of structural properties like the concentration index (CI; Fig. 10e) and the SDSS deVAB_r index (Fig. 10f). Inspection of SDSS images corroborates the similarities between PGs and RGs, most of which are ellipticals, although some of the RGs turn out to be spirals (as can be deduced by the tail towards low CI in Fig. 10e), including an apparently higher than normal rate of edge-on systems. An investigation of this issue is beyond the scope of this paper, but we note that this ‘contaminant’ population tends to have $W_{\text{H}\alpha}$ close to the RG/wAGN frontier, and thus may be related to the unavoidable fuzziness of classification schemes.

In terms of luminosity-weighted mean stellar ages (Fig. 10g), sAGN are younger than wAGN, which in turn are younger than RGs and PGs. From Fig. 7 we infer that the tail of RGs towards smaller mean ages is due to systems at the RG/wAGN border. The mean stellar metallicities (Fig. 10h) are similar for all types, with a tail of sAGN reaching lower values.

The distributions of stellar extinctions (Fig. 10i) show a distinct $\text{PG} < \text{RG} < \text{wAGN} < \text{sAGN}$ pattern. To double-check this result, Fig. 10(l) shows the distribution of $\text{H}\alpha/\text{H}\beta$, but only for sources where this ratio is reliable, a criterion which excludes PGs and most RGs. Despite its incompleteness, Fig. 10(l) confirms that wAGN have higher extinction than RGs and lower than sAGN. The class with the lowest extinction is the SF class, in spite of the intense star formation which is usually associated with high extinction. The underlying reason for a smaller extinction in SF than the rest of galaxies lies in their lower masses (see Stasińska et al. 2004; Garn & Best 2010). Regarding the $\text{PG} \rightarrow \text{RG} \rightarrow \text{wAGN} \rightarrow \text{sAGN}$ extinction sequence, its interpretation is not straightforward, since it involves the dust mass and distribution, as well as its composition (dust grains recently produced by the progenitors of HOLMES and expected to be found in RGs do not have the same extinction properties as grains processed in the interstellar medium and associated with regions of star formation).

Fig. 10(j) shows the distribution of ξ uncorrected for dust. The $\text{PG} \rightarrow \text{RG} \rightarrow \text{wAGN} \rightarrow \text{sAGN} \rightarrow \text{SF}$ sequence reflects the central role of $W_{\text{H}\alpha}$ in our classification scheme. This sequence is mirrored in the distribution of observed $\text{H}\alpha$ luminosities (Fig. 10k). PGs included in these panels have, by definition, very weak $\text{H}\alpha$ (median $W_{\text{H}\alpha} = 0.23 \text{ \AA}$, and median $S/\text{N}_{\text{H}\alpha} = 2.4$ counting only those with an $\text{H}\alpha$ flux in our data base). Still, their locations in these diagrams are consistent with them not being completely lineless.

8 DISCUSSION AND SUMMARY

The goal of this paper was to provide a comprehensive classification of galaxies according to their emission-line properties which would be able to cope with the large population of weak line galaxies that do not appear in traditional diagrams (e.g. BPT) because they lack some of the diagnostic lines. This is possible using the WHAN diagram ($W_{\text{H}\alpha}$ versus $[\text{N II}]/\text{H}\alpha$) that we proposed in earlier work (CF10). An additional problem with the BPT diagram and other similar line-ratio diagrams is that, as shown by S08, the LINER region contains a mix of two completely different families of galaxies: galaxies that contain a wAGN and ‘RGs’, i.e. galaxies that have stopped forming stars and whose emission lines are powered by their HOLMES. A truly comprehensive classification scheme must account for this phenomenon, and the WHAN diagram allows so.

To distinguish true AGN from fake ones (i.e. the RGs), we have shown that a useful criterion is the value of ξ , which measures the intrinsic extinction-corrected $\text{H}\alpha$ luminosity in units of the $\text{H}\alpha$ luminosity expected from stellar populations older than 10^8 yr uncovered by our stellar population analysis software STARLIGHT. In principle, ξ should be equal to 1 if the galaxy absorbs all the ionizing photons provided by its HOLMES, and > 1 if any other source of ionization is present. We have shown that this index is bimodally distributed, with a $\xi \gg 1$ population composed by galaxies undergoing vigorous star formation and/or nuclear activity, and a population of galaxies centred right at the predicted value for RGs. Computing ξ for each galaxy, however, is not a trivial task: it requires a stellar population analysis able to identify the populations of HOLMES and a recipe to obtain the ionizing radiation field from these HOLMES. The latter strongly depends on how the (yet quite uncertain) evolutionary

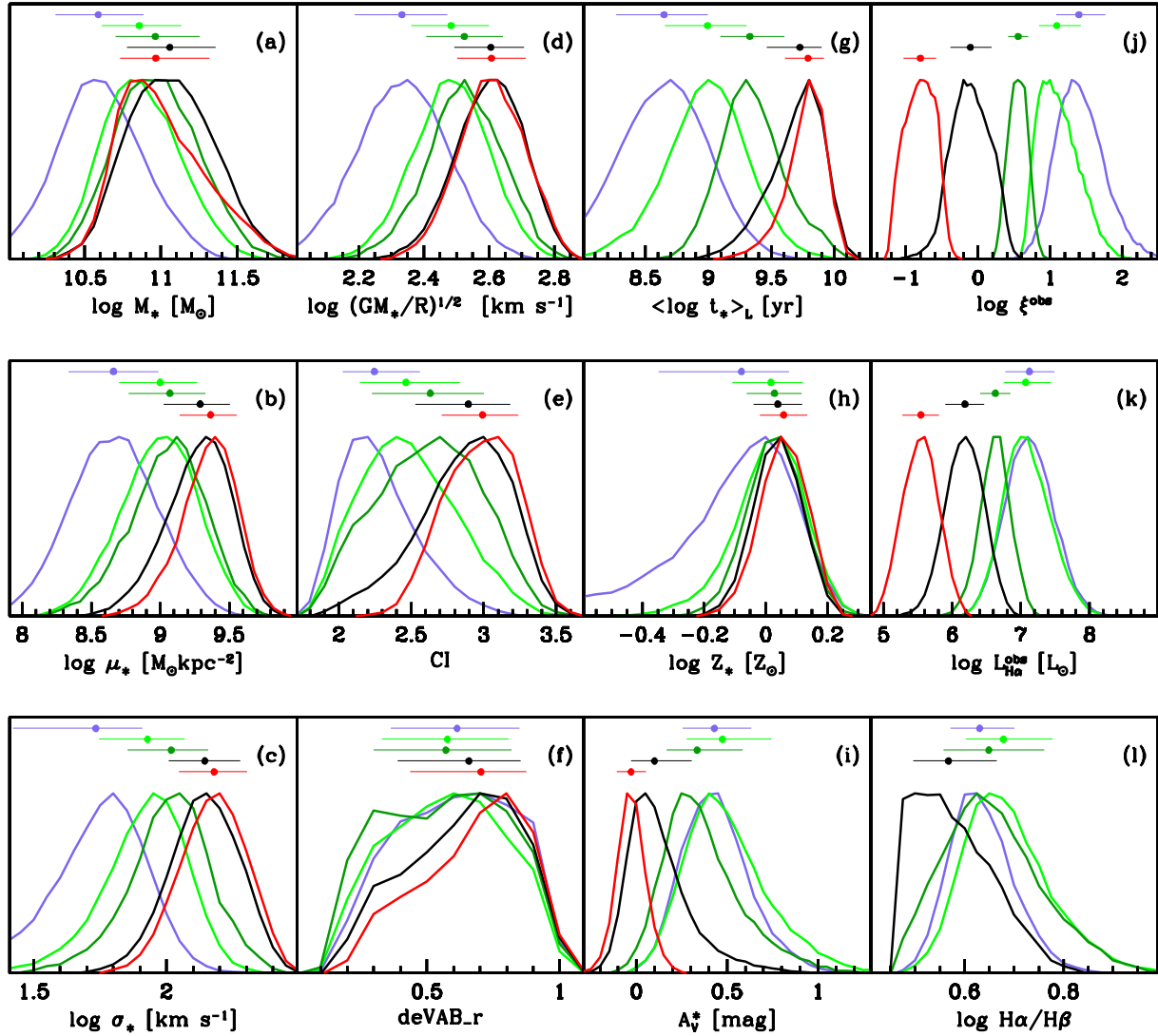


Figure 10. Normalized histograms of properties for different galaxy classes. Colours code the SF, sAGN, wAGN, RG and PG classes as in Fig. 6. Horizontal bars trace the 16 to 84 percentile ranges, with the median marked by a circle, with the vertical shifts ordered as SF (top), sAGN, wAGN, RG and PG (bottom). All galaxies from our volume-limited sample are included, except for panel (l), for which a reliable $H\alpha/H\beta$ was required, hence excluding all PGs and most RGs.

tracks for post-asymptotic giant branch stars are incorporated into the stellar population codes as well as on other issues such as the IMF and the metallicities of the stellar populations.

It is therefore preferable to base the distinction between true and fake AGN on the $H\alpha$ equivalent width, an easy to obtain observational parameter which provides an excellent proxy for ξ . In view of the strong dichotomy in the observed $W_{H\alpha}$ distribution for galaxies in the right wing of the BPT diagram (i.e. the wing previously supposed to contain only AGN), we propose a practical separation between wAGN and RGs based on a class frontier at $W_{H\alpha} = 3 \text{ \AA}$. This physically inspired but data-guided separation corresponds to the minimum between the two modes in the $W_{H\alpha}$ distribution.

We thus identify five classes of galaxies in the WHAN diagram:

- (i) SF: pure star-forming galaxies: $\log[N \text{ II}]/H\alpha < -0.4$ and $W_{H\alpha} > 3 \text{ \AA}$;
- (ii) sAGN: strong AGN (i.e. Seyferts): $\log[N \text{ II}]/H\alpha > -0.4$ and $W_{H\alpha} > 6 \text{ \AA}$;

- (iii) wAGN: weak AGN: $\log[N \text{ II}]/H\alpha > -0.4$ and $3 < W_{H\alpha} < 6 \text{ \AA}$;
- (iv) RG: retired galaxies (i.e. fake AGN): $W_{H\alpha} < 3 \text{ \AA}$;
- (v) PG: passive galaxies (actually, lineless galaxies): $W_{H\alpha}$ and $W_{[N \text{ II}]} < 0.5 \text{ \AA}$.

Note that the border between RGs and PGs is somewhat arbitrary, but this is not really a concern.

We have then analysed the SFHs of the different classes of galaxies, as well as the distribution of a dozen of physical or observational properties, such as the galaxy stellar mass M_* , surface densities μ_* , velocity dispersions σ_* and stellar extinctions A_V^* obtained through STARLIGHT. All these comparisons corroborate our proposed differentiation between RGs and wAGN in the LINER-like family. We also find that wAGN have properties overlapping with those of sAGN, while RGs line up with PGs. In other words, wAGN are the low-activity end of the AGN family, while RGs are PGs with emission lines. As a matter of fact, both RGs and PGs are ‘retired’ or

‘passive’ galaxies, the real spectroscopic difference between them being the presence or absence of emission lines. It is only the inherited custom which imposed the adopted nomenclature.

Now that these emission-line classes have been established, further work could be to understand what is at the root of the strength of the AGN phenomenon or why some PGs present emission lines and others do not.

ACKNOWLEDGMENTS

The STARLIGHT project is supported by the Brazilian agencies CNPq, CAPES, by the France–Brazil CAPES–COFECUB programme, and by Observatoire de Paris.

Funding for the SDSS and SDSS-II has been provided by the Alfred P. Sloan Foundation, the Participating Institutions, the National Science Foundation, the US Department of Energy, the National Aeronautics and Space Administration, the Japanese Monbukagakusho, the Max Planck Society and the Higher Education Funding Council for England. The SDSS website is <http://www.sdss.org/>.

The SDSS is managed by the Astrophysical Research Consortium for the Participating Institutions. The Participating Institutions are the American Museum of Natural History, Astrophysical Institute Potsdam, University of Basel, University of Cambridge, Case Western Reserve University, University of Chicago, Drexel University, Fermilab, the Institute for Advanced Study, the Japan Participation Group, Johns Hopkins University, the Joint Institute for Nuclear Astrophysics, the Kavli Institute for Particle Astrophysics and Cosmology, the Korean Scientist Group, the Chinese Academy of Sciences (LAMOST), Los Alamos National Laboratory, the Max-Planck-Institute for Astronomy (MPIA), the Max-Planck-Institute for Astrophysics (MPA), New Mexico State University, Ohio State University, University of Pittsburgh, University of Portsmouth, Princeton University, the United States Naval Observatory and the University of Washington.

REFERENCES

Abazajian K. N. et al., 2009, *ApJS*, 182, 543
 Annibali F., Bressan A., Rampazzo R., Zeilinger W. W., Vega O., Panuzzo P., 2010, *A&A*, 519, A40
 Asari N. V., Cid Fernandes R., Stasińska G., Torres-Papaqui J. P., Mateus A., Sodré L., Schoenell W., Gomes J. M., 2007, *MNRAS*, 381, 263
 Baldwin J. A., Phillips M. M., Terlevich R., 1981, *PASP*, 93, 5
 Bamford S. P., Rojas A. L., Nichol R. C., Miller C. J., Wasserman L., Genovese C. R., Freeman P. E., 2008, *MNRAS*, 391, 607
 Binette L., Magris C. G., Stasińska G., Bruzual A. G., 1994, *A&A*, 292, 13
 Blanton M. R., Moustakas J., 2009, *ARA&A*, 47, 159
 Bloeker T., 1995, *A&A*, 299, 755
 Bressan A., Fagotto F., Bertelli G., Chiosi C., 1993, *A&AS*, 100, 647
 Brinchmann J., Charlot S., White S. D. M., Tremonti C., Kauffmann G., Heckman T., Brinkmann J., 2004, *MNRAS*, 351, 1151
 Bruzual G., Charlot S., 2003, *MNRAS*, 344, 1000 (BC03)
 Cardelli J. A., Clayton G. C., Mathis J. S., 1989, *ApJ*, 345, 245
 Chabrier G., 2003, *PASP*, 115, 763
 Charbonnel C., Meynet G., Maeder A., Schaerer D., 1996, *A&AS*, 115, 339
 Cid Fernandes R., González Delgado R. M., 2010, *MNRAS*, 403, 780
 Cid Fernandes R., Mateus A., Sodré L., Stasińska G., Gomes J. M., 2005, *MNRAS*, 358, 363
 Cid Fernandes R., Stasińska G., Schlickmann M. S., Mateus A., Vale Asari N., Schoenell W., Sodré L., 2010, *MNRAS*, 403, 1036 (CF10)
 Connolly A. J., Szalay A. S., Bershadsky M. A., Kinney A. L., Calzetti D., 1995, *AJ*, 110, 1071

Coziol R., Ribeiro A. L. B., de Carvalho R. R., Capelato H. V., 1998, *ApJ*, 493, 563
 de Grijs M. H. K., Keel W. C., Miley G. K., Goudfrooij P., Lub J., 1992, *A&AS*, 96, 389
 de Vaucouleurs G., 1960, *AJ*, 65, 51
 Eracleous M., Hwang J. A., Flohic H. M. L. G., 2010, *ApJ*, 711, 796
 Fioc M., Rocca-Volmerange B., 1997, *A&A*, 326, 950
 Folkes S. R., Lahav O., Maddox S. J., 1996, *MNRAS*, 283, 651
 Garn T., Best P., 2010, *MNRAS*, 409, 421
 González Delgado R. M., Cid Fernandes R., Pérez E., Martins L. P., Storchi-Bergmann T., Schmitt H., Heckman T., Leitherer C., 2004, *ApJ*, 605, 127
 Harris W., 1996, *AJ*, 112, 1487
 Heckman T. M., 1980, *A&A*, 87, 142
 Hills J. G., 1972, *A&A*, 17, 155
 Hubble E. P., 1936, *Realm of the Nebulae*. Yale Univ. Press, New Haven
 Kauffmann G. et al., 2003, *MNRAS*, 346, 1055
 Kaviraj S., 2010, *MNRAS*, 406, 382
 Kewley L. J., Groves B., Kauffmann G., Heckman T., 2006, *MNRAS*, 372, 961
 Koleva M., Prugniel P., Ocvirk P., Le Borgne D., Soubiran C., 2008, *MNRAS*, 385, 1998
 Kroupa P., 2001, *MNRAS*, 322, 231
 Lejeune T., Cuisinier F., Buser R., 1997, *A&AS*, 125, 229
 Lintott C. et al., 2010, *ArXiv e-prints*
 Lyon J., 1975, *ApJ*, 201, 168
 Macchetto F., Pastoriza M., Caon N., Sparks W. B., Giavalisco M., Bender R., Capaccioli M., 1996, *A&AS*, 120, 463
 Masters K. L. et al., 2010, *MNRAS*, 405, 783
 Mateus A., Sodré L., Cid Fernandes R., Stasińska G., Schoenell W., Gomes J. M., 2006, *MNRAS*, 370, 721
 Miller C. J., Nichol R. C., Gómez P. L., Hopkins A. M., Bernardi M., 2003, *ApJ*, 597, 142
 Mollá M., García-Vargas M. L., 2000, *A&A*, 359, 18
 Mollá M., García-Vargas M. L., Bressan A., 2009, *MNRAS*, 398, 451
 Morgan W. W., Mayall N. U., 1957, *PASP*, 69, 291
 Ocvirk P., 2010, *ApJ*, 709, 88
 Pastoriza M., 1968, *Bol. Asociacion Argentina Astron. La Plata Argentina*, 14, 7
 Rauch T., 2003, *A&A*, 403, 709
 Salpeter E. E., 1955, *ApJ*, 121, 161
 Sánchez Almeida J., Muñoz-Tuñón C., Amorín R., Aguerri J. A., Sánchez-Janssen R., Tenorio-Tagle G., 2008, *ApJ*, 685, 194
 Sánchez Almeida J., Aguerri J. A. L., Muñoz-Tuñón C., de Vicente A., 2010, *ApJ*, 714, 487
 Sarzi M. et al., 2010, *MNRAS*, 402, 2187
 Schaller G., Schaerer D., Meynet G., Maeder A., 1992, *A&AS*, 96, 269
 Schawinski K. et al., 2010, *ApJ*, 711, 284
 Schoenberger D., 1983, *ApJ*, 272, 708
 Smith H. E., Lonsdale C. J., Lonsdale C. J., 1998, *ApJ*, 492, 137
 Sodré L., Jr, Cuevas H., 1994, *Vistas Astron.*, 38, 287
 Sokolowski J., Bland-Hawthorn J., 1991, *PASP*, 103, 911
 Stasińska G., Mateus A., Jr, Sodré L., Jr, Szczerba R., 2004, *A&A*, 420, 475
 Stasińska G., Cid Fernandes R., Mateus A., Sodré L., Asari N. V., 2006, *MNRAS*, 371, 972 (S06)
 Stasińska G., Vale Asari N., Cid Fernandes R., Gomes J. M., Schlickmann M., Mateus A., Schoenell W., Sodré L., Jr, 2008, *MNRAS*, 391, L29 (S08)
 Strauss M. A. et al., 2002, *AJ*, 124, 1810
 Terzian Y., 1974, *ApJ*, 193, 93
 York D. G. et al., 2000, *AJ*, 120, 1579

This paper has been typeset from a \LaTeX file prepared by the author.